Biomedical and Pharmaceutical Sciences
Faculty Publications

Biomedical and Pharmaceutical Sciences

2013

A Comparative Study of Hollow Copper Sulfide Nanoparticles and Hollow Gold Nanospheres on Degradability and Toxicity

Laingran Guo
University of Rhode Island

Irene Panderi

Daisy D. Yan
University of Rhode Island

Kevin Szulak
University of Rhode Island

Yajuan Li
University of Rhode Island

Follow this and additional works at: https://digitalcommons.uri.edu/bps_facpubs

This is a pre-publication author manuscript of the final, published article.

Terms of Use
This article is made available under the terms and conditions applicable towards Open Access
Policy Articles, as set forth in our Terms of Use.

Authors

Laingran Guo, Irene Panderi, Daisy D. Yan, Kevin Szulak, Yajuan Li, Yi-Tzai Chen, Hang Ma, Daniel B. Niesen, Navindra P. Seeram, Aftab Ahmed, Bingfang Yan, Dionysios Pantazatos, and Wei Lu

A Comparative Study of Hollow Copper Sulfide Nanoparticles and Hollow Gold Nanospheres on Degradability and Toxicity

Liangran Guo[†], **Irene Panderi**[‡,⊥], **Daisy D. Yan**[†], **Kevin Szulak**[†], **Yajuan Li**[†], **Yi-Tzai Chen**[†], **Hang Ma**[†], **Daniel B. Niesen**[†], **Navindra Seeram**[†], **Aftab Ahmed**[†], **Bingfang Yan**[†], **Dionysios Pantazatos**[‡,§], and **Wei Lu**[†,‖,*]

[†]Department of Biomedical and Pharmaceutical Sciences, College of Pharmacy, The University of Rhode Island, Kingston, Rhode Island 02881, United States

[‡]COBRE Center for Cancer Research and Development, Rhode Island Hospital, Rhode Island 02903, United States

[§]Warren Alpert Medical School, Brown University, Providence, Rhode Island 02903, United States

[⊥]Department of Pharmacy, Division of Pharmaceutical Chemistry, University of Athens, Panepistimiopolis, Zografou, Athens 15771, Greece

[‖]School of Pharmacy, Fudan University, Shanghai 201203, China

Abstract

Gold and copper nanoparticles have been widely investigated for photothermal therapy of cancer. However, degradability and toxicity of these nanoparticles remain concerns. Here, we compare hollow CuS nanoparticles (HCuSNPs) with hollow gold nanospheres (HAuNS) in similar particle sizes and morphology following intravenous administration to mice. The injected pegylated HCuSNPs (PEG-HCuSNPs) are eliminated through both hepatobiliary (67 percentage of injected dose, %ID) and renal (23 %ID) excretion within one month post injection. By contrast, 3.98 %ID of Au is excreted from liver and kidney within one month after i.v. injection of pegylated HAuNS (PEG-HAuNS). Comparatively, PEG-HAuNS are almost non-metabolizable, while PEG-HCuSNPs are considered biodegradable nanoparticles. PEG-HCuSNPs do not show significant toxicity by histological or blood chemistry analysis. Principal component analysis and 2-D peak distribution plots of data from matrix-assisted laser desorption ionization-time of flight imaging mass spectrometry (MALDI-TOF IMS) of liver tissues demonstrated a reversible change in the proteomic profile in mice receiving PEG-HCuSNPs. This is attributed to slow dissociation of Cu ion from CuS nanoparticles along with effective Cu elimination for maintaining homeostasis. Nonetheless, an irreversible change in the proteomic profile is observed in the liver from mice receiving PEG-HAuNS by analysis of MALDI-TOF IMS data, probably due to the non-metabolizability of Au. This finding correlates with the elevated serum lactate dehydrogenase at 3 months after PEG-HAuNS injection, indicating potential long-term toxicity. The comparative

[*]Corresponding author: Department of Biomedical and Pharmaceutical Sciences, College of Pharmacy, The University of Rhode Island, 7 Greenhouse Road, Kingston, Rhode Island 02881, USA. Phone: +1-401-874-5517. Fax: +1-401-874-5787. weilu@uri.edu.

Conflict of Interest: The authors declare no competing financial interest.

Supporting Information Available: A549 cell viability after NIR laser irradiation; thermographic images of nude mice bearing A549 xenografts following various photothermal treatments; photographs of mouse urine following i.v. injection of PEG-HCuSNPs or PEG-HAuNS; TEM/EDS analysis of HCuSNPs and SCuSNPs in plasma and urine; cumulative release of Cu ions from PEG-HCuSNPs in PBS; workflow for MALDI-TOF IMS analysis; difference in average mass spectra of liver in mice after various treatments. This material is available free of charge *via* the Internet at http://pubs.acs.org.

results between the two types of nanoparticles will advance the development of HCuSNPs as a new class of biodegradable inorganic nanomaterials for photothermal therapy.

Keywords

hollow CuS nanoparticles (HCuSNPs); hollow gold nanospheres (HAuNS); degradability; toxicity; matrix-assisted laser desorption ionization-time of flight imaging mass spectrometry (MALDI-TOF IMS)

The design and synthesis of multi-functional nanomaterials have provided potential applications in biomedical fields such as molecular imaging and drug delivery. Interest in using inorganic nanostructures such as gold and CuS nanoparticles has surged in the last decades as these particles exhibit strong optical absorption at near-infrared (NIR) wavelengths (650–900 nm). They convert optical energy into thermal energy, and deposit benign NIR optical energy into tumors for thermal ablation of tumor cells.[1–8] Gold nanostructures (nanoshells,[1] nanorods,[2] nanocages,[3] and hollow nanospheres[4]) are widely reported as photothermal coupling agents to enhance the efficacy of photothermal therapy. Although the metallic gold nanoparticles with bioinert properties show great promise for clinical applications,[9, 10] they are non-biodegradable, raising concerns regarding their long-term metabolism.[11–13]

Semiconductor CuS nanoparticles (CuSNPs) are a class of inorganic photo-absorbers that provide an alternative to gold analogs. CuSNPs with particle sizes 3 nm[5] and 11 nm,[6, 14] flower-like CuS superstructures (~1 μm in diameter),[7] and Cu_9S_5 plate-like nanocrystals (~70 nm × 13 nm)[8] have intense optical absorption at NIR region. In contrast to exogenous gold, copper is essential for human health.[15] In adults, the highest safe intake level of Cu is 10 mg daily,[16] indicating that CuS nanoparticles may be metabolized by humans. However, critical pharmacological parameters such as body disposition and long-term metabolism of these CuSNPs remain unknown. Moreover, there is a paucity of data regarding the cytotoxicity profile of the CuSNPs.[5, 8] This knowledge is essential for clinical applications of CuS nanomaterials.

In this study, we compared degradability and toxicity between the two types of photothermal nanoparticles, *i.e.* hollow gold nanospheres (HAuNS)[17] and hollow CuS nanoparticles (HCuSNPs),[18] in mice following systemic administration. The two nanoparticles were formulated with similar particle size and morphology. They were both surface-modified with polyethylene glycol (PEG) in order to evade uptake by monophagocytic systems. Therefore, their pharmacokinetics and disposition were contingent on the intrinsic characteristics of the nanoparticles such as crystal structures and chemical composition. In addition to routine toxicity evaluation, matrix-assisted laser desorption ionization (MALDI)-time of flight (TOF) imaging mass spectrometry (IMS) was employed to analyze changes in the molecular profile of liver in mice before and after the injection. Understanding the fate and toxicity profile of these two nanoparticles *in vivo* will provide valuable information designing biodegradable and safe inorganic nanomaterials for photothermal therapy.

RESULTS AND DISCUSSION

Transmission electron microscopy (TEM) illustrated that HCuSNPs (~70 nm) and HAuNS (~50 nm) were morphologically similar; both were spherical shape and hollow interiors (Figures 1A and 1B). Their particle size distributions were both in the range of 50 – 100 nm, consistent with favorable pharmacokinetics and enhanced permeability and retention effect in tumor following systemic administration.[19] Both nanoparticles displayed intense optical

absorbance in the NIR region (Figure 1C). Following pegylation, at equivalent mass concentrations (*i.e.* 27 μg/mL of Cu or Au), PEG-HCuSNPs and PEG-HAuNS had similar absorption intensities at 900 nm (0.48 *v.s.* 0.52 A.U.). Because of the similarity of the particles in morphology and absorption at 900 nm, PEG-HCuSNPs and PEG-HAuNS exhibited identical photothermal ablation effect on cancer cells upon 900-nm NIR laser treatment (Figure S1). In nude mice bearing A549 human lung adenocarcinoma xenografts, real-time infrared thermal imaging illustrates that the temperature of tumor area in mice pretreated with PEG-HCuSNPs (20 mg/kg of Cu) or PEG-HAuNS (20 mg/kg of Au) elevates to 53°C at 1 min after the laser irradiation with power intensity of 2.0 W/cm^2 (Figure S2). These results suggest that PEG-HCuSNPs and PEG-HAuNS have similar efficacies of photothermally induced tumor destruction, since elevation of temperature to 51°C for 100 s can cause irreversible thermal damage to cells or tissues.[20, 21]

To compare their fate *in vivo*, we first examined the biodistribution of Cu or Au in major organs after a single i.v. injection of PEG-HCuSNPs or PEG-HAuNS in BALB/c mice. Both liver and spleen retained larger amounts of Cu or Au than other organs during the entire 3-month postinjection period (Figure 2A). The accumulation of the two nanoparticles in liver and spleen at 1 day could be attributed to short term effect of the pegylation.[22] PEG modification of both nanoparticles is likely to take effect during the first few hours after administration, while the PEG coating may disappear thereafter based on chain length and charged groups of the PEG molecules.[22, 23] Intriguingly, the Cu level in liver decreased much faster than Au level after 1 day. The Cu level in liver was 1.1 ± 0.1 percentage of injected dose per gram (%ID/g) at 3 months after injection of PEG-HCuSNPs, which was only 5% of the amount at 1 day postinjection (Figure 2B). However, the injected PEG-HAuNS remained 11.4 ± 1.8 %ID/g in liver after 3 month, which was 70% of the amount at 1 day postinjection. Similar accumulation profile was found in the spleen. At 3 months postinjection, there was 6.9% of Cu remaining in spleen compared to 1-day's level. In contrast, 94.6% of the injected PEG-HAuNS remained after 3 months. The Cu levels in lung, kidney and heart also decreased much faster than the Au levels (Figure 2A). There was no retention of Cu in all major organs except liver or spleen after 3 months, while a significant amount of Au in major organs remained. The distribution results demonstrated that the PEG-HCuSNPs were efficiently eliminated from the body.

To understand how HCuSNPs were cleared from the body, we collected urine up to one month following i.v. injection. Interestingly, the urine collected following injection of PEG-HCuSNPs was noticeably greenish (Figure S3, green arrows). Following high speed centrifugation (15,871 g, 15 min), a dark green pellet was observed, whereas the supernatant turned yellow (Figure S3, blue arrows). This result prompted us to hypothesize that some CuSNPs were excreted from the kidney, since CuSNPs appear green in aqueous solution. However, the original structure of HCuSNPs was not detected under TEM of the urine sample collected at 24 h following PEG-HCuSNPs injection. Instead, there were a few small CuS nanoparticles (SCuSNPs) in the urine (Figure 3A, arrows). TEM at higher magnification revealed particles with crystal lattice structures of 3–5 nm in diameter (Figure 3A, inlets, arrows). HCuSNPs were composed of hexagonal CuS crystals with an average crystalline size of 12.5 nm, calculated by the Debye-Scherrer formula.[24] Our TEM imaging illustrated that the shell of HCuSNPs was porous and composed of small particles of 11–12 nm in diameter (Figure 3B, arrow). This observation was in line with formation of the HCuSNPs by the Kirkendall effect.[24] The CuSNPs were formed on the outside and inside surfaces of the CuS shell through sulfidation. The produced CuS shell was a poly-crystalline structure, and the holes in the shell became a shortcut for mass diffusion and transference.[24] We thus presumed that the porous CuS shell structure may facilitate its disintegration *in vivo*. Imaging of pellets from plasma collected at 3 h postinjection of PEG-HCuSNPs indicated that most HCuSNPs were intact (Figure 3C). However, there were a small number

of SCuSNPs with particle sizes of 4–5 nm visualized in the same pellet (Figures 3D and 3E, arrows). Energy dispersion spectrum (EDS) analysis confirmed that these small particles observed in the urine and plasma were CuS crystallites with similar Cu-to-S atomic ratio to HCuSNPs (Figure S4). Since the effective size cutoff of glomerular filtration was 10 nm for the rapid renal clearance of small nanoparticles such as gold nanoparticles and quantum dots,[25–27] and since the size and composition of the SCuSNPs disintegrated in the plasma was in agreement with that observed in the urine (3–5 nm), we concluded that a small number of PEG-HCuSNPs disintegrated into SCuSNPs in blood, followed by directly renal excretion.

Quantitative analysis of Cu in urine including supernatant (Cu ions) and pellet (SCuSNPs) in the 1-month study delineated a continuous renal excretion following i.v. injection of PEG-HCuSNPs (Figure 4A). The cumulative Cu excreted from the kidney was 22.7 ± 6.6 percentage of injected dose (%ID), of which the amount of Cu in form of SCuSNPs only accounted for 4.8%. The Cu ion (95.2%) was the dominant form in the urine. This result supported our TEM observation that only small amounts of SCuSNPs appeared in plasma. Renal excretion of Cu in both particulate and ionic forms displayed a two-phase elimination profile (Figure 4A), an initial fast excretion phase (0 – 12 h) followed by secondary slow excretion phase (12 h – 30 d). Ionic Cu presumably was the product of degradation and/or biotransformation of HCuSNPs or the protein-bound SCuSNPs. This result correlated with the fast elimination of Cu in the major organs, evidencing that the HCuSNPs can be metabolized in the body.

In contrast, analysis of Au in urine following i.v. injection of PEG-HAuNS showed very little renal excretion of Au (Figure 4B). The cumulative Au excreted from the kidney was only 0.08 ± 0.02 %ID throughout 1 month postinjection. There was no discernible gold nanocrystal in urine under TEM imaging (data not shown), although trace amounts of Au were detected in the urine pellet. The very slow elimination rate of HAuNS indicated that PEG-HAuNS are almost non-metabolizable.

We looked further into the liver distribution of both PEG-HCuSNPs and PEG-HAuNS, since liver uptake was the highest among all the investigated organs. Histochemistry with silver staining was utilized to visualize CuSNPs. The CuSNPs were converted into silver sulfide particles that exhibited black contrasts under white field light microscopy. As shown in Figure 5A, there were two forms of CuSNPs present in liver at 1 day postinjection of PEG-HCuSNPs. The majority were agglomerates or large aggregates of the nanoparticles. The rest were single or small particle aggregates (Figure 5A, 1 d, upper image). Co-staining with the macrophage-specific marker, CD68,[28] demonstrated that the black agglomerates formed in liver macrophages (brown staining) – Kupffer cells (Figure 5A, 1 d, lower image). On the other hand, the small particles were sporadically distributed in either liver interstitium or hepatocytes. At 1 week postinjection, these small particles almost disappeared without significant accumulation in hepatocytes (Figure 5A, 1 w, lower image). The number of nanoparticle-loaded Kupffer cells, as well as the number of agglomerates in each Kupffer cell, also decreased with time. After 1 month, only a few agglomerates were found in a small population of Kupffer cells (Figure 5A, 1 m, lower image, arrow). After 3 months, almost no agglomerates were observed in the liver. This result indicated that the elimination of CuSNPs in liver may be attributed to Cu metabolism by the hepatocytes through hepatobiliary excretion.[29] Quantitative analysis of Cu in feces proved that 66.9 ± 27.2 %ID of Cu was excreted through the bile within 1 month post-injection (Figure 6A). Collectively, the Cu elimination through both renal and hepatobiliary excretion was calculated to be almost 90 %ID within one month following injection of PEG-HCuSNPs.

For evaluation of the distribution of HAuNS, we observed the scattering of gold nanoparticles under dark field light microscopy.[30] At 1 day following injection of PEG-HAuNS, the distribution pattern of gold nanoparticles in liver was found to be similar to that of the CuSNPs (Figure 5B). However, the elimination of gold in liver was much slower than that of Cu, as evidenced by significant amounts of gold agglomerates observed in Kupffer cells after 3 months. The Au excretion from the bile was 3.9 ± 1.8 %ID within 1 month post-injection (Figure 6B). The total Au elimination from both kidney and liver was only 3.98 %ID within 1 month post-injection.

It was reported that the biodegradable poly(DL-lactide-co-glycolide) (PLGA) microspheres with 50% and 26% of glycolic acid content injected intramuscularly in rats degraded *in vivo* with half-lives of 2 weeks and 12 weeks, respectively.[31] In terms of biodegradable mesoporous silica nanoparticles, half of the nanoparticles were cleared from the body at 4 weeks post i.v. injection.[32] Our results demonstrated that about 90% of the PEG-HCuSNPs were eliminated from mice within one month following i.v. injection. Compared with the PLGA microspheres and mesoporous silica nanoparticles, the PEG-HCuSNPs were cleared faster. PEG-HCuSNPs thus can be considered to be biodegradable nanoparticles. In contrast, the elimination of 40-nm colloidal gold nanoparticles in liver in C57BL mice was reportedly very slow, with only a 9% fall in the gold content over 6 months following i.v. injection.[12] The calculated daily elimination rate was only 0.05%. By extrapolation, a large fraction of injected gold nanoparticles will remain in the liver even beyond the normal mouse lifespan.[12] In another report, accumulation of 20-nm gold nanoparticles in liver and spleen in Wistar rats did not decrease after two months.[13] Our results here agree with these observations, indicating gold nanoparticles are almost non-metabolizable or with extremely long elimination half-lives.

A proposed disposition profile of PEG-HCuSNPs following i.v. injection is shown in Scheme 1. The major population of blood-circulating PEG-HCuSNPs distributes into tissues where the HCuSNPs gradually disintegrate into SCuSNPs, further dissociating Cu ions. The Cu ions are eliminated through both hepatobiliary and renal excretion. Within one month after administration, about 67% of the injected Cu is eliminated through the bile, and 23% through the urine. Of the renally excreted Cu, the majority (95.2%) is ionic as a result of degradation and biotransformation of HCuSNPs or the protein-bound SCuSNPs. The rest (4.8%) is in SCuSNP form. These SCuSNPs are directly excreted from the kidney during the initial elimination phase (0–12 h postinjection), and they presumably have specific zwitterionic coating accessible to urinary excretion rather than forming protein coronas.[27]

We next examined the cytotoxicity of PEG-HCuSNPs and PEG-HAuNS by a 3-(4,5-dimethylthiazol-2-yl)-2,5-diphenyltetrazolium bromide (MTT) assay of mouse macrophage RAW264.7 cells and primarily cultured mouse hepatocytes.[33, 34] We did not observe a significantly inhibitory effect of PEG-HCuSNPs or PEG-HAuNS on cell proliferation at a Cu or Au concentration range of 3.2–100 μg/mL (Figure 7A). Since excessive tissue accumulation of Cu ions is known to cause toxicity, we investigated the cytotoxicity of free Cu ions. The cell viability was reduced to 35.6% on RAW264.7 cells and 43.3% on mouse hepatocytes when treated with $CuCl_2$ solution at a Cu concentration of 100 μg/mL, respectively. Because the solubility product constant K_{sp} of CuS is 7.9×10^{-37} at 25°C, only 3.2 ± 0.3% of Cu ions were released from the PEG-HCuSNPs in the medium within 24 h (Figure S5). The low toxicity of PEG-HCuSNPs thus appears to be due to the slow dissociation rate of Cu ions from CuS. This is supported by the previous report of Cu_9S_5 nanocrystals displaying a very low cytotoxicity at concentration of 100 ppm on HeLa cells due to only 3.7 ppm of Cu ions released.[8]

Following i.v. injection of a single dose of PEG-HCuSNPs or PEG-HAuNS (20 mg/kg of Cu or Au per mouse), there were no deaths in any of the experimental groups during the 3-month period. The mice treated with PEG-HCuSNPs did not show significant increase in any tested serum biochemical parameters compared to the control mice without any treatment (Figure 7B). This result indicated that a single dose of PEG-HCuSNPs did not impair liver or kidney function. Comparatively, there was a noticeable elevation of serum lactate dehydrogenase (LDH) in mice at 3 months after injection of PEG-HAuNS, although other biochemical parameters remained normal levels (Figure 7B). This finding implied that the injection of PEG-HAuNS possibly caused certain long-term toxic effect. Nonetheless, H&E staining of the liver did not show any apparent change in cellular structures after PEG-HCuSNPs or PEG-HAuNS injection during the 3-month study (Figure 7C).

In order to understand the effect of these nanoparticles on the body and to determine whether any resulting changes occurred in the molecular content in tissues, we employed MALDI-TOF IMS to characterize the differences in the molecular profile of frozen liver tissue sections from BALB/c mice treated with a single i.v. injection of PEG-HCuSNPs or PEG-HAuNS. In MALDI-TOF IMS analysis, a laser ablated a 20–80 μm spot radius of tissue upon which the desorbed ionized proteins were detected using TOF mass spectrometry and were represented as individual mass peaks in the acquired spectrum (see Figure S6 workflow). Each mass spectrum contained information of the molecular composition of one spot. The mass spectra generated at each x, y coordinate were exported using FlexImaging software for profile analysis, which identified unique differences in tissue heterogeneity at a spectral (Figure S7) and spatial level (imaging of mass peaks), respectively. The spectral and spatial differences indicated presence or absence, co-localization or de-localization of specific proteins. As shown in Figure S7, the average spectra from the samples after the i.v. administration of PEG-HCuSNPs or PEG-HAuNS exhibited variations of peak distribution and intensity as compared to samples without treatment (Control) over time. More importantly, the spectral profiles between the CuS and Au nanoparticles in the tissue were significantly different indicating remarkable distinction in the molecular composition within the cells.

To further evaluate this spectral difference, we imported the spectra of each tissue sample (group) into ClinProTools software for statistical analysis.[35] Using ClinProTools, p value of t-test analysis of variance (ANOVA) and difference average analysis were performed to analyze the peak intensity difference in order to rank a series of differentiated peaks between the nanoparticle-treated samples and the control. The 2-D peak distribution views were used to display the distribution of the two most significant peaks among the ranking lists (See Supporting Information for 2-D Peak Distribution approach). In PEG-HCuSNPs-treated samples, peaks at 8566 Da and at 4964 Da were identified as the two most statistically significant peaks according to a p-value t-test ANOVA list (Figure 8A). Peaks at 4964 Da and at 3458 Da were identified as the two most statistically significant peaks based on a difference average test (Figure 8B). The 2-D peak distribution plots of these two-peak sets both demonstrated that the distribution of the liver samples at 1 day (pink ellipse) after injection of PEG-HCuSNPs departed from that of blank control (blue ellipse). The maximum variations were observed at 7 days (red ellipse) after the administration that did not overlap with other samples. Nonetheless, after 3 months the distribution tended to return to normal levels with some overlap between green and blue ellipses.

As MALDI-TOF IMS collects sequential spectra from spots over the entire tissue section, information on spatial distribution of all the biomolecules can be obtained. To identify such change at a spatial level, the above mass peaks (3458 Da, 4964 Da and 8566 Da) were mapped on the tissue to visualize their distribution and relative abundance (Figure 8C). The spatial distribution of each of these peaks illustrated significant decreases in intensity and

varying distribution patterns 1 day after the injection of PEG-HCuSNPs compared with that of control. The intensity was further diminished after 7 days. However, the expression of these molecules returned close to normal levels after 3 months. The results from 2-D peak distribution plots and mass peak imaging clearly demonstrated a reversible difference in these statistically significant peaks that differentiated between the PEG-HCuSNPs-injected and control samples. This trend can be representative of the spectral profile of the nanoparticle-treated samples.

To confirm this trend, we used another statistical method, principle component analysis (PCA), for identifying the significantly differential peaks in the spectral data (See Supporting Information for PCA approach). This approach has been outlined for the analysis of proteomic profiles of cancer patients and biomarker identification.[35, 36] The score output (Figure 8D, top row) demonstrated distinction between the PEG-HCuSNPs-injected and control samples in the three principal component (PC) coordinates. From plots of PC1 *v.s.* PC2, and PC2 *v.s.* PC3, it was apparent that PC2 accounted for the trend in the distribution of variation of the peaks. After the injection of PEG-HCuSNPs the distribution of the PC scores at 1 day (pink dots) or 7 days (red dots) displayed significant deviation from that of the control (blue dots) along PC2 axis. Nonetheless, after 3 months the distribution along PC2 axis returned to near normal (green dots *v.s.* blue dots). The PCA result further substantiated a reversible variance in the proteomic profile of liver following i.v. injection of PEG-HCuSNPs.

In PEG-HAuNS-treated samples, the 2-D peak distribution plots of peaks (4737 Da, 4964 Da) and peaks (4964 Da, 14970 Da) identified using the t-test ANOVA list (Figure 9A) and difference average list (Figure 9B), respectively, depicted departure of peak distributions of the sample at 1 day after the injection from that of the control. The variations at 7 days after the injection reached a maximum. There was no distribution (ellipse) overlap between the samples at 3 months after the injection and the control, although the difference slightly reduced between them as shown in Figure 9B. Mass peak imaging also showed the variations in expression of these identified differential peaks (4737 Da, 4964 Da and 14970 Da) at 1 day, 7 days, or 3 months after the injection (Figure 9C). However, the signals of peaks at 4737 Da and at 14970 Da did not tend to be restored to normal levels after 3 months. The spatial distribution of peak at 4964 remained heterogeneity after 3 months compared with that of control. In addition, as shown in PCA score output (Figure 9D, top row), the distribution patterns of PC1, PC2 or PC3 at 1 day (pink dots), 7 days (red dots), or 3 months (green dots) after PEG-HAuNS injection were significantly different from those of the control (blue dots). These data delineated an irreversible change in the proteomic profile of the liver following i.v. injection of PEG-HAuNS.

MALDI-TOF IMS is a molecular imaging technology that adds a dimension to classical proteomics analysis by providing information on the spatial distribution of biomolecules (*e.g.* proteins, peptides, lipids, metabolites) in a tissue section.[37–40] MALDI-TOF IMS offers several key advantages including extreme sensitivity, capture of all biomolecular content in a single spectrum, and production of as many ion maps as the number of detected peaks in the mass spectrum for one acquisition step. Most importantly, there is no need for prerequisite knowledge on the molecules to be analyzed by MALDI-TOF IMS.[39, 41] Because of these advantages, applications of MALDI-TOF IMS have rapidly grown in the biomedical research field such as diagnosis and prognosis through analysis and classification of tissue samples by their proteomic profile.[39, 42–44] We, here, applied the MALDI-TOF IMS to nanotoxicity evaluation through analyzing difference between normal and nanoparticle-treated liver tissues at a molecular level. Our measurements generated important information that was complementary to traditional methods of histopathologic and blood chemistry analysis. First, MALDI-TOF IMS were able to detect subtle changes of

biomolecules in liver tissue. In both PEG-HCuSNPs and PEG-HAuNS treated liver samples, variations of proteomic profile by 2-D peak distribution plot, mass peak imaging or PCA plot were clearly detected, while no significantly histological changes were observed by the H&E staining analysis. Second, results from MALDI-TOF IMS analysis correlated with the nanoparticle distribution in liver over time. The variations shown in both mass peak imaging and plots of statistical analysis at 1 day after injection of the nanoparticles were a result of singnificant accumulation of the nanoparticles in liver. After 7 days, large amounts of the remaining nanoparticles in liver produced a cumulative effect on the proteomic profile, reaching a maximum variation compared to the normal control. Since 95% of the liver-distributed Cu was eliminated at 3 months after injection of PEG-HCuSNPs, the proteomic profile tended to return to normal levels. In contrast, because 70% of PEG-HAuNS remained in the liver at 3 months after injection, the molecular profile was not likely to be restored to normal. Third, changes of biomolecules in liver detected by MALDI-TOF IMS mirrored the pharmacologic and toxicity effect of the nanoparticles. The reversible variations of the liver proteomic profile following injection of PEG-HCuSNPs were in line with the data of the blood chemistry analysis, substantiating biodegradability as well as little or no toxicity of the particles. Nonetheless, an irreversible change in the liver proteomic profile at 3 months after injection of PEG-HAuNS correlated with the elevated serum LDH level, indicating non-metabolizability and potential long-term toxicity of PEG-HAuNS. Accordingly, the MALDI-TOF IMS of liver tissues is an accurate and sensitive tool for the evaluation of nanotoxicity *in vivo*. This method can be applied to evaluating the toxicity of any other nanoparticles. Future experiments will be performed to identify those altered biomolecules.

Although Cu is an essential trace element in the body, free Cu ions in excess are toxic. We have demonstrated little or no toxicity of PEG-HCuSNPs at a single dose of 20 mg/kg Cu. This is because CuS has very small solubility product constant (7.9×10^{-37}). The slow dissociation of Cu ions, along with effective elimination of Cu ions,[45] are believed to maintain homeostasis without drastically increased toxicity. The level of Cu ions is tightly regulated by several transporters and chaperones.[46] These proteins also prevent cellular damage from an excess accumulation of Cu by mediating the efflux of Cu from the cell. Intracellularly, several proteins such as copper-transporting ATPases, as well as metallothionein (MT)[47–49] and glutathione (GSH)[50] are complexed with Cu, representing intracellular transport, storage or detoxication of these ions. Further investigation will focus on the expression levels of these proteins as well as the Cu excretion mechanisms.

Gold nanoparticles generally show little or no acute toxicity because the bulk material is bioinert. The HAuNS in this study was synthesized under citrate stabilization, followed by replacement with neutral PEG.[17] Without introduction of the cationic ligands to the HAuNS, histological analysis of PEG-HAuNS-treated mice showed no significantly structural change of the liver cells. However, an elevated serum LDH level as well as irreversible change in the proteomic profile of the liver at 3 months post-injection in this study, suggested need for further investigation of the potential long-term toxicity of PEG-HAuNS. This result was consistent with the previous finding that the i.v. injected gold nanoparticles caused changes of gene expression in the liver and spleen ascribed to the non-metabolizable properties of gold.[13]

CONCLUSIONS

In summary, this study specified biodegradability of PEG-HCuSNPs that was distinct from non-metabolizability of PEG-HAuNS. The comparative results between the two types of nanoparticles revealed that the nanotoxicity was tightly related to the degradability of the nanoparticles. The current findings advance further studies on design of biodegradable and safe PEG-HCuSNPs for photothermal therapy in clinics. Moreover, we for the first time

explored the MALDI-TOF IMS to evaluate nanotoxicity, which determined changes in the molecular composition of liver tissues administered with nanoparticles. The information obtained from proteomic profiling by MALDI-TOF IMS complements results from conventional toxicity test, providing a comprehensive understanding of nanotoxicity.

EXPERIMENTAL SECTION

Materials

The chemicals used were purchased from Sigma-Aldrich Chemical, Inc. unless mentioned specifically. BALB/c mice (both 6–8 weeks, male and female) were ordered from Charles River Laboratories International, Inc. All animal experiments were conducted in compliance with the guidelines for the care and use of research animals established by the University of Rhode Island Institutional Animal Care and Use Committee (IACUC).

Nanoparticles synthesis and characterization

HCuSNPs were synthesized according to our previously reported method.[18] The HCuSNPs were centrifuged at 15,557 g for 15 min at room temperature, and washed twice with distilled water. After resuspended in 4.8 mL of water, the nanoparticles were mixed with 200 μL of PEG-SH (5 mg/mL, MW 5,000) for 12 h at room temperature to obtain PEG-HCuSNPs. The nanoparticles were then centrifuged, and washed twice with distilled water. The HAuNS were synthesized and pegylated according to the previous report.[17] The nanoparticles were deposited on the grid and directly examined under the TEM (JEOL JEM2100). The absorbance spectrum was measured by DU800 UV/Vis spectrophotometer (Beckman Coulter). The nanoparticles were dissolved in aqua regia for the inductively coupled plasma mass spectrometer (ICP-MS) (Model: X7, Thermo Electron Corporation) quantitative analysis of Cu or Au.[51]

Biodistribution of nanoparticles in BALB/c mice

BALB/c mice were divided into ten experimental groups (5 mice per group). PEG-HCuSNPs (20 mg/kg of Cu) or PEG-HAuNS (20 mg/kg of Au) were injected through tail vein. Mice were sacrificed at 1 day, 1 week, 2 weeks, 1 month and 3 months post injection. Blood was withdrawn, and tissues including heart, liver, spleen, lung and kidney were collected for ICP-MS analysis. Half of liver tissue in each group was cryosectioned for histological analysis.

For ICP-MS analysis, the tissue samples were digested using a Mars 5 microwave system (CEM Corporation). In brief, approximately 20 mg of tissue samples were weighed and transferred into digestion vessels. After adding 1 mL of nitric acid to each vessel, the samples were digested for 10 min with the power of 600 W. Afterwards, 0.2 mL of digested solution was added to 9.8 mL of deionized water for ICP-MS analysis. The calibration standards of Cu and Au in four concentrations (0, 50, 100, and 200 ng/mL) were analyzed with each batch of samples. The average recovery efficiencies of Cu and Au were 98 – 102 %.

For histological analysis of CuS nanoparticles in liver, the tissues were fixed with 4% paraformaldehyde at room temperature for 20 min. A 5.0% silver nitrate aqueous solution was prepared as solution A. An aqueous solution containing 2% hydroquinone and 5% citric acid was prepared as solution B. After rinsed with deionized water, the slices were developed in freshly filtered solution of 1 part A and 5 parts B for 3 min. Following deionized water washing, the slices were counterstained with hematoxylin. In separate slices, following sliver staining, antigen was retrieved by proteinase K for 10 min at room temperature. The slices were stained with rat anti-mouse CD68 monoclonal antibody (1:100,

AbD SeroTec) at 4°C overnight, followed by peroxidase-goat anti-rat IgG (1:200, Life Technologies) for 1 h at room temperature. The samples were developed using diaminobenzidine tetrahydrochloride (DAB) kit (Life Technologies) according to the manufacturer's suggested protocol followed by hematoxylin counterstaining.

For histological analysis of distribution of HAuNS in liver, the proteinase K treated slices were stained with rat anti-mouse CD68 monoclonal antibody (1:100) followed by Alexa Fluor 594-conjugated goat anti-rat IgG (Life Technologies) for 1 h at room temperature. The cell nuclei were counterstained with 4′,6-diamidino-2-phenylindole (DAPI). The slices were examined under the Nikon fluorescence microscope equipped with a dark field condenser.

Urine and feces sample collection and analysis

BALB/c mice were randomly divided into 2 groups (n=3). The mice were i.v. injected with PEG-HCuSNPs (20 mg/kg of Cu) or PEG-HAuNS (20 mg/kg of Au). The mice were then transferred to mouse metabolic cages (Tecniplast) for urine and feces collection up to one month. Another 3 mice without injection were used as control. The mice were allowed to access food and water freely. The urine samples were centrifuged at 15,871 g for 15 min to separate the pellet and supernatant. Both urine and feces samples were digested as the above described method for analysis of Cu or Au content.

For TEM imaging, urine samples collected 24 h following nanoparticles injection, were directly deposited on the grid without counterstaining. For TEM analysis of blood sample, the blood was withdrawn 3 h after i.v. injection of PEG-HCuSNPs (20 mg/kg of Cu). The blood was transferred to Eppendorf tube with heparin. Plasma was collected after centrifugation at 845 g for 5 min. The pellet containing nanoparticles was separated from the plasma by further centrifugation at 15,871 g for 15 min. Resuspended in water, the plasma pellet was deposited on the grid without counterstaining.

In vitro cytotoxicity

Murine macrophage RAW264.7 cells (ATCC) were seeded in 96-well plate at a density of 10,000 cells per well and incubated for 24 h to allow the cells to attach. The cells were exposed to PEG-HCuSNPs, or PEG-HAuNS, or $CuCl_2$ with various Cu or Au concentrations in DMEM plus 10% FBS. After 24 h, cell viability was measured using the MTT assay according to the manufacturer suggested procedures. The data represented the means of quadruplicate measurements.

In a separate study, primary hepatocytes were isolated from BALB/c mice by our modified two-step collagenase digestion method.[33] Washed with Williams' Medium E for three times, the hepatocytes were suspended in same medium containing 35% percoll. The resulting cell pellet was then suspended in Williams' Medium E containing 10% FBS, insulin transferrin-sodium selenite (ITS) supplement, and dexamethasone (100 nM). Cell viability was determined by trypan blue exclusion. Hepatocytes were plated onto collagen-coated 96-well culture plates at a density of 10,000 cells per well. The cells were allowed to attach for 4 h at 37°C. Culture plates were then gently swirled, and the medium containing unattached cells was aspirated. Same fresh medium was added.[34] After 2 d, the cells were exposed to PEG-HCuSNPs, or PEG-HAuNS, or $CuCl_2$ with different Cu or Au concentrations in the same medium. After 24 h, cell viability was measured using the MTT assay.

Blood biochemistry and histology

Male BALB/c mice were randomly divided into 7 groups (n = 5). The mice received an i.v. injection of PEG-HCuSNPs (20 mg/kg of Cu) or PEG-HAuNS (20 mg/kg of Au). Blood samples were collected at 7 day, 1 month or 3 months after nanoparticle injection for

chemical analysis. Mice without treatment were used as control. For histological evaluation, portions of the liver collected were fixed in 10% buffered formalin-saline at 4 °C overnight and then embedded in paraffin blocks. Tissue sections (5-μm thickness) were stained with hematoxylin and eosin (H&E).

MALDI-TOF IMS analysis

Tissue sections of 5 μm were applied onto ITO (Indium Teen Oxide) one-side coated, conductive glass slides. A matrix solution (synapic acid, 10 mg/mL in ACN/TFA 0.2%, 6:4, v/v) was then applied using Image Prep (Bruker Daltonics). Spectra were collected across the entire tissue area using the Ultraflex III MALDI-TOF/TOF instrument (Bruker Daltonics) with a SmartBeam laser operating at 100 Hz in linear mode over a mass range of m/z 2,000 to 20,000. A laser spot diameter of 100 nmu;m and a raster width of 100 μm were used. Using the FlexImaging software (Bruker Daltonics), teaching points were generated to ensure the correct positioning of the laser for spectral acquisition. The software exports the specific geometry of the tissue to be analyzed, and an instrument-specific automated method is created, which generates a grid across the tissue of spots where the laser will acquire data. Calibration was done externally using a protein standard mixture in the mass range of m/z 6,000 to 16,500. The intensity of each signal over the entire mass range acquired is plotted as a function of location on the tissue, allowing the visualization of the location of each m/z detected. These images were generated and visualized using FlexImaging software. Consequently, the spectra derived from regions of interest in each tissue were exported using the FlexImaging software for profile analysis. Normalizing, baseline subtracting, peak defining and comparison of multiple spectra were performed automatically using ClinProtTools software. PCA and 2-D peak distribution were managed by an external MATLAB software tool, which was integrated in ClinProTools.

Supplementary Material

Refer to Web version on PubMed Central for supplementary material.

Acknowledgments

References

1. Lal S, Clare SE, Halas NJ. Nanoshell-Enabled Photothermal Cancer Therapy: Impending Clinical Impact. Acc Chem Res. 2008; 41:1842–1851. [PubMed: 19053240]

2. Alkilany AM, Thompson LB, Boulos SP, Sisco PN, Murphy CJ. Gold Nanorods: Their Potential for Photothermal Therapeutics and Drug Delivery, Tempered by the Complexity of Their Biological Interactions. Adv Drug Deliv Rev. 2012; 64:190–199. [PubMed: 21397647]

3. Xia Y, Li W, Cobley CM, Chen J, Xia X, Zhang Q, Yang M, Cho EC, Brown PK. Gold Nanocages: From Synthesis to Theranostic Applications. Acc Chem Res. 2011; 44:914–924. [PubMed: 21528889]

4. Melancon MP, Zhou M, Li C. Cancer Theranostics with near-Infrared Light-Activatable Multimodal Nanoparticles. Acc Chem Res. 2011; 44:947–956. [PubMed: 21848277]

5. Li Y, Lu W, Huang Q, Huang M, Li C, Chen W. Copper Sulfide Nanoparticles for Photothermal Ablation of Tumor Cells. Nanomedicine (Lond). 2010; 5:1161–1171. [PubMed: 21039194]

6. Zhou M, Zhang R, Huang M, Lu W, Song S, Melancon MP, Tian M, Liang D, Li C. A Chelator-Free Multifunctional [^{64}Cu]CuS Nanoparticle Platform for Simultaneous Micro-Pet/Ct Imaging and Photothermal Ablation Therapy. J Am Chem Soc. 2010; 132:15351–15358. [PubMed: 20942456]

7. Tian Q, Tang M, Sun Y, Zou R, Chen Z, Zhu M, Yang S, Wang J, Wang J, Hu J. Hydrophilic Flower-Like Cus Superstructures as an Efficient 980 Nm Laser-Driven Photothermal Agent for Ablation of Cancer Cells. Adv Mater. 2011; 23:3542–3547. [PubMed: 21735487]

8. Tian Q, Jiang F, Zou R, Liu Q, Chen Z, Zhu M, Yang S, Wang J, Hu J. Hydrophilic Cu9s5 Nanocrystals: A Photothermal Agent with a 25. 7% Heat Conversion Efficiency for Photothermal Ablation of Cancer Cells *in Vivo*. ACS Nano. 2011; 5:9761–9771. [PubMed: 22059851]

9. Pilot Study of Aurolase(Tm) Therapy in Refractory and/or Recurrent Tumors of the Head and Neck. http://clinicaltrials.gov/show/NCT00848042

10. Efficacy Study of Aurolase Therapy in Subjects with Primary and/or Metastatic Lung Tumors. http://clinicaltrials.gov/show/NCT01679470

11. Sharifi S, Behzadi S, Laurent S, Forrest ML, Stroeve P, Mahmoudi M. Toxicity of Nanomaterials. Chem Soc Rev. 2012; 41:2323–2343. [PubMed: 22170510]

12. Sadauskas E, Danscher G, Stoltenberg M, Vogel U, Larsen A, Wallin H. Protracted Elimination of Gold Nanoparticles from Mouse Liver. Nanomedicine. 2009; 5:162–169. [PubMed: 19217434]

13. Balasubramanian SK, Jittiwat J, Manikandan J, Ong CN, Yu LE, Ong WY. Biodistribution of Gold Nanoparticles and Gene Expression Changes in the Liver and Spleen after Intravenous Administration in Rats. Biomaterials. 2010; 31:2034–2042. [PubMed: 20044133]

14. Ku G, Zhou M, Song S, Huang Q, Hazle J, Li C. Copper Sulfide Nanoparticles as a New Class of Photoacoustic Contrast Agent for Deep Tissue Imaging at 1064 Nm. ACS Nano. 2012; 6:7489–7496. [PubMed: 22812694]

15. Uriu-Adams JY, Keen CL. Copper, Oxidative Stress, and Human Health. Mol Aspects Med. 2005; 26:268–298. [PubMed: 16112185]

16. Http://Des.Nh.Gov/Organization/Commissioner/Pip/Factsheets/Ard/Documents/Ard-Ehp-9.Pdf

17. Lu W, Xiong C, Zhang G, Huang Q, Zhang R, Zhang JZ, Li C. Targeted Photothermal Ablation of Murine Melanomas with Melanocyte-Stimulating Hormone Analog-Conjugated Hollow Gold Nanospheres. Clin Cancer Res. 2009; 15:876–886. [PubMed: 19188158]

18. Ramadan S, Guo L, Li Y, Yan B, Lu W. Hollow Copper Sulfide Nanoparticle-Mediated Transdermal Drug Delivery. Small. 2012; 8:3143–3150. [PubMed: 22829400]

19. Li SD, Huang L. Pharmacokinetics and Biodistribution of Nanoparticles. Mol Pharm. 2008; 5:496–504. [PubMed: 18611037]

20. Welch AJ. The Thermal Response of Laser Irradiated Tissue. IEEE J Quantum Electron. 1984; 20:1471–1481.

21. Diederich CJ. Thermal Ablation and High-Temperature Thermal Therapy: Overview of Technology and Clinical Implementation. Int J Hyperthermia. 2005; 21:745–753. [PubMed: 16338857]

22. Lipka J, Semmler-Behnke M, Sperling RA, Wenk A, Takenaka S, Schleh C, Kissel T, Parak WJ, Kreyling WG. Biodistribution of Peg-Modified Gold Nanoparticles Following Intratracheal Instillation and Intravenous Injection. Biomaterials. 2010; 31:6574–6581. [PubMed: 20542560]

23. Jokerst JV, Lobovkina T, Zare RN, Gambhir SS. Nanoparticle Pegylation for Imaging and Therapy. Nanomedicine (Lond). 2011; 6:715–728. [PubMed: 21718180]

24. Zhu H, Wang J, Wu D. Fast Synthesis, Formation Mechanism, and Control of Shell Thickness of Cus Hollow Spheres. Inorg Chem. 2009; 48:7099–7104. [PubMed: 19585979]

25. Choi CH, Zuckerman JE, Webster P, Davis ME. Targeting Kidney Mesangium by Nanoparticles of Defined Size. Proc Natl Acad Sci U S A. 2011; 108:6656–6661. [PubMed: 21464325]

26. Choi HS, Ipe BI, Misra P, Lee JH, Bawendi MG, Frangioni JV. Tissue- and Organ-Selective Biodistribution of Nir Fluorescent Quantum Dots. Nano Lett. 2009; 9:2354–2359. [PubMed: 19422261]

27. Choi HS, Liu W, Misra P, Tanaka E, Zimmer JP, Itty Ipe B, Bawendi MG, Frangioni JV. Renal Clearance of Quantum Dots. Nat Biotechnol. 2007; 25:1165–1170. [PubMed: 17891134]

28. Lu W, Huang Q, Ku G, Wen X, Zhou M, Guzatov D, Brecht P, Su R, Oraevsky A, Wang LV, et al. Photoacoustic Imaging of Living Mouse Brain Vasculature Using Hollow Gold Nanospheres. Biomaterials. 2010; 31:2617–2626. [PubMed: 20036000]

29. Mercer JF, Llanos RM. Molecular and Cellular Aspects of Copper Transport in Developing Mammals. J Nutr. 2003; 133:1481S–1484S. [PubMed: 12730448]

30. Melancon MP, Lu W, Yang Z, Zhang R, Cheng Z, Elliot AM, Stafford J, Olson T, Zhang JZ, Li C. *In Vitro* and *in Vivo* Targeting of Hollow Gold Nanoshells Directed at Epidermal Growth Factor Receptor for Photothermal Ablation Therapy. Mol Cancer Ther. 2008; 7:1730–1739. [PubMed: 18566244]

31. Shive MS, Anderson JM. Biodegradation and Biocompatibility of Pla and Plga Microspheres. Adv Drug Deliv Rev. 1997; 28:5–24. [PubMed: 10837562]

32. Liu T, Li L, Teng X, Huang X, Liu H, Chen D, Ren J, He J, Tang F. Single and Repeated Dose Toxicity of Mesoporous Hollow Silica Nanoparticles in Intravenously Exposed Mice. Biomaterials. 2011; 32:1657–1668. [PubMed: 21093905]

33. Shi D, Yang D, Yan B. Dexamethasone Transcriptionally Increases the Expression of the Pregnane X Receptor and Synergistically Enhances Pyrethroid Esfenvalerate in the Induction of Cytochrome P450 3a23. Biochem Pharmacol. 2010; 80:1274–1283. [PubMed: 20599767]

34. Yang D, Yang J, Shi D, Xiao D, Chen YT, Black C, Deng R, Yan B. Hypolipidemic Agent Z-Guggulsterone: Metabolism Interplays with Induction of Carboxylesterase and Bile Salt Export Pump. J Lipid Res. 2012; 53:529–539. [PubMed: 22246918]

35. Shao C, Tian Y, Dong Z, Gao J, Gao Y, Jia X, Guo G, Wen X, Jiang C, Zhang X. The Use of Principal Component Analysis in Maldi-Tof Ms: A Powerful Tool for Establishing a Mini-Optimized Proteomic Profile. Am J Biomed Sci. 2012; 4:85–101. [PubMed: 22229059]

36. Ketterlinus R, Hsieh SY, Teng SH, Lee H, Pusch W. Fishing for Biomarkers: Analyzing Mass Spectrometry Data with the New Clinprotools Software. Biotechniques. 2005; (Suppl):37–40. [PubMed: 16528916]

37. Cho YT, Su H, Huang TL, Chen HC, Wu WJ, Wu PC, Wu DC, Shiea J. Matrix-Assisted Laser Desorption Ionization/Time-of-Flight Mass Spectrometry for Clinical Diagnosis. Clin Chim Acta. 2013; 415:266–275. [PubMed: 23089072]

38. Caldwell RL, Caprioli RM. Tissue Profiling by Mass Spectrometry: A Review of Methodology and Applications. Mol Cell Proteomics. 2005; 4:394–401. [PubMed: 15677390]

39. Cornett DS, Reyzer ML, Chaurand P, Caprioli RM. Maldi Imaging Mass Spectrometry: Molecular Snapshots of Biochemical Systems. Nat Methods. 2007; 4:828–833. [PubMed: 17901873]

40. Alexandrov T. Maldi Imaging Mass Spectrometry: Statistical Data Analysis and Current Computational Challenges. BMC Bioinformatics. 2012; 13(Suppl 16):S11. [PubMed: 23176142]

41. Andersson M, Groseclose MR, Deutch AY, Caprioli RM. Imaging Mass Spectrometry of Proteins and Peptides: 3d Volume Reconstruction. Nat Methods. 2008; 5:101–108. [PubMed: 18165806]

42. Wisztorski M, Croix D, Macagno E, Fournier I, Salzet M. Molecular Maldi Imaging: An Emerging Technology for Neuroscience Studies. Dev Neurobiol. 2008; 68:845–858. [PubMed: 18383549]

43. Chaurand P, Cornett DS, Caprioli RM. Molecular Imaging of Thin Mammalian Tissue Sections by Mass Spectrometry. Curr Opin Biotechnol. 2006; 17:431–436. [PubMed: 16781865]

44. Wisztorski M, Lemaire R, Stauber J, Menguelet SA, Croix D, Mathe OJ, Day R, Salzet M, Fournier I. New Developments in Maldi Imaging for Pathology Proteomic Studies. Curr Pharm Des. 2007; 13:3317–3324. [PubMed: 18045185]

45. Arredondo M, Nunez MT. Iron and Copper Metabolism. Mol Aspects Med. 2005; 26:313–327. [PubMed: 16112186]

46. Furukawa T, Komatsu M, Ikeda R, Tsujikawa K, Akiyama S. Copper Transport Systems Are Involved in Multidrug Resistance and Drug Transport. Curr Med Chem. 2008; 15:3268–3278. [PubMed: 19075668]

47. Weiner AL, Cousins RJ. Copper Accumulation and Metabolism in Primary Monolayer Cultures of Rat Liver Parenchymal Cells. Biochim Biophys Acta. 1980; 629:113–125. [PubMed: 7370303]

48. Webb M, Cain K. Functions of Metallothionein. Biochem Pharmacol. 1982; 31:137–142. [PubMed: 7037006]

49. Bremner I, Beattie JH. Metallothionein and the Trace Minerals. Annu Rev Nutr. 1990; 10:63–83. [PubMed: 2200476]

50. Freedman JH, Ciriolo MR, Peisach J. The Role of Glutathione in Copper Metabolism and Toxicity. J Biol Chem. 1989; 264:5598–5605. [PubMed: 2564391]

51. Cheng K, Peng S, Xu C, Sun S. Porous Hollow Fe_3O_4 Nanoparticles for Targeted Delivery and Controlled Release of Cisplatin. J Am Chem Soc. 2009; 131:10637–10644. [PubMed: 19722635]
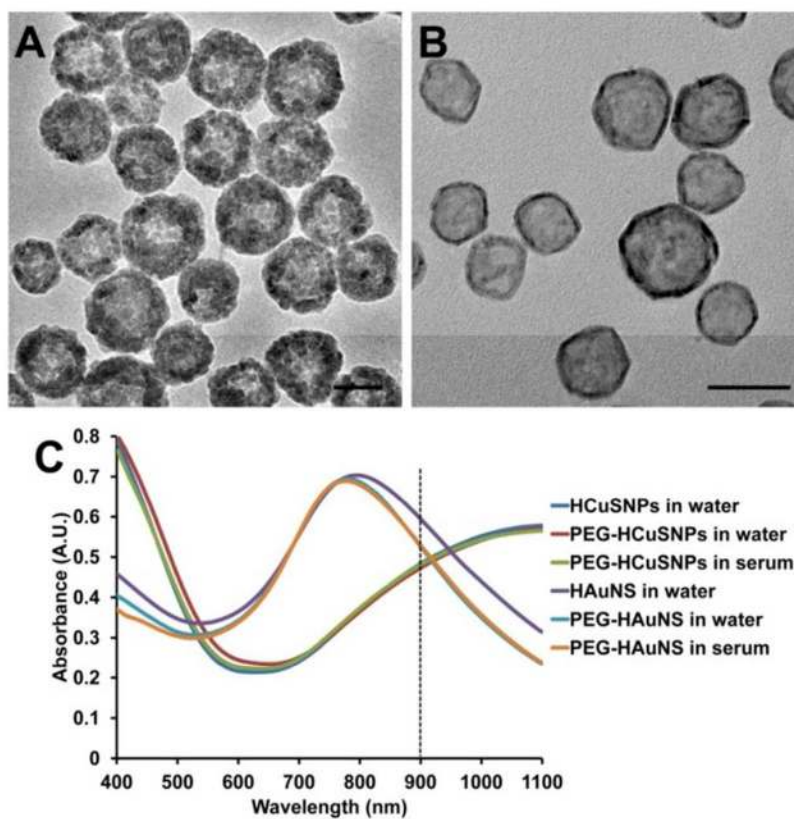
Figure 1.
TEM of (A) HCuSNPs and (B) HAuNS. Bars, 50 nm. (C), Experimental absorbance spectra of the nanoparticles (27 µg/mL of Cu or Au) in water or mouse serum.
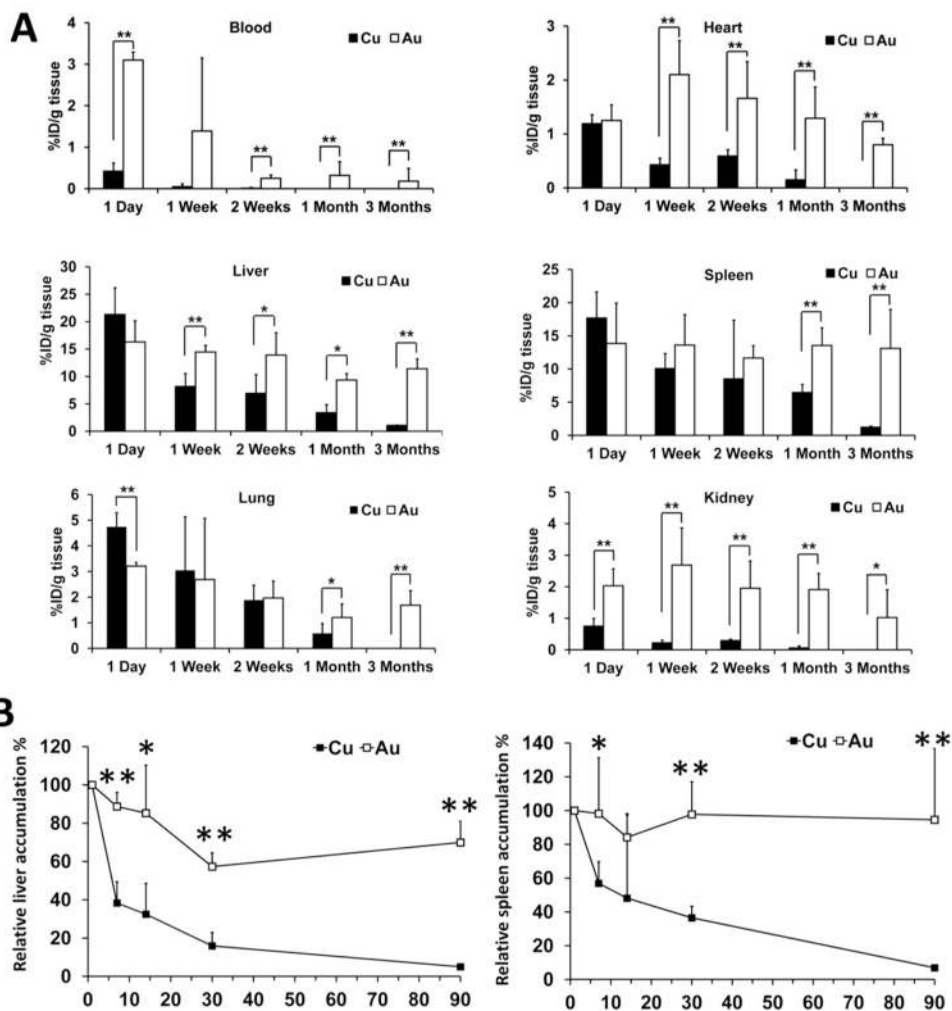
Figure 2.
(A), Biodistribution of Cu or Au in BALB/c mice following i.v. injection of PEG-HCuSNPs (20 mg/kg of Cu) or PEG-HAuNS (20 mg/kg of Au). Data are expressed as percentage of injected dose per gram of tissue (%ID/g tissue) and are presented as mean ± standard deviation (n=5). *, *P* < 0.05; **, *P* < 0.01 for %ID/g of Cu *v.s.* %ID/g of Au. (B), Relative liver and spleen accumulation of Cu or Au postinjection. Data are expressed as percentage of Cu or Au accumulation compared to 1-day postinjection groups and are presented as mean ± standard deviation (n=5). *, *P* < 0.05; **, *P* < 0.01 for relative accumulation of Cu *v.s.* that of Au.
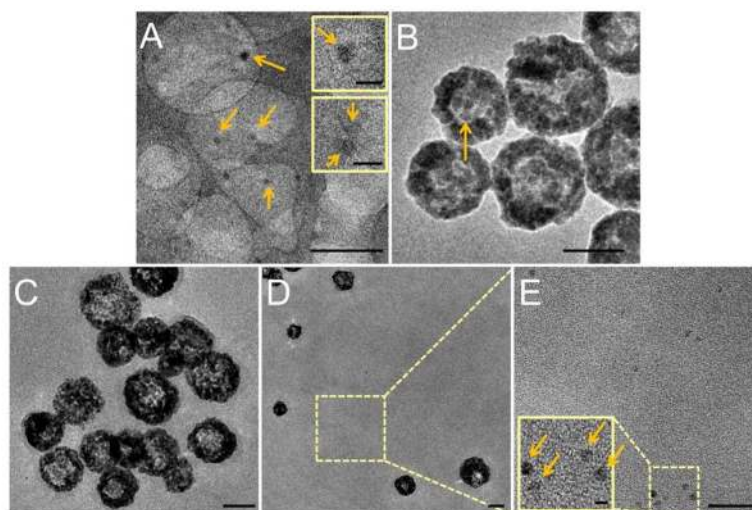
Figure 3.
Renal excretion of PEG-HCuSNPs. (A), TEM of small CuS nanoparticles (SCuSNPs, arrows) in urine collected from BALB/c mice at 24 h following i.v. injection of PEG-HCuSNPs. (B), TEM of HCuSNPs in water. Arrow, small CuS crystalline structure. (C–E), TEM of CuS nanoparticles separated from plasma at 3 h following i.v. injection of PEG-HCuSNPs. Most CuS nanoparticles were intact PEG-HCuSNPs (C), while there were a few SCuSNPs (D and E, arrows). Bars, A–E, 50 nm; inlet bars, 5 nm.
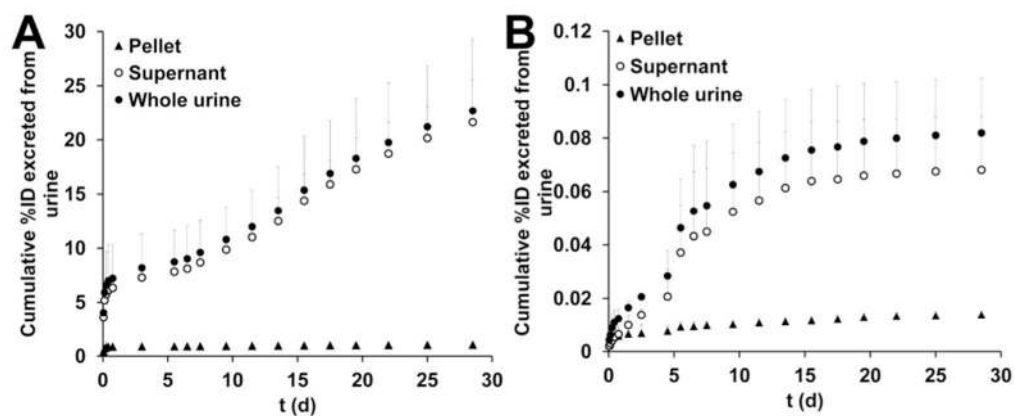
Figure 4.
Cumulative renal excretion of Cu (A) and Au (B) from mice injected with PEG-HCuSNPs (20 mg/kg of Cu) or PEG-HAuNS (20 mg/kg of Au). The "t" of X-axis represents the median time between the starting and ending time points of each urine sample collection. Each urine sample was separated into pellet and supernatant by high speed centrifugation (15,871 g, 15 min). The total amount of Cu or Au of each urine sample was the sum of the amount in pellet and that in supernatant. %ID represents percentage of injected dose. Data are presented as mean ± standard deviation (n=3).
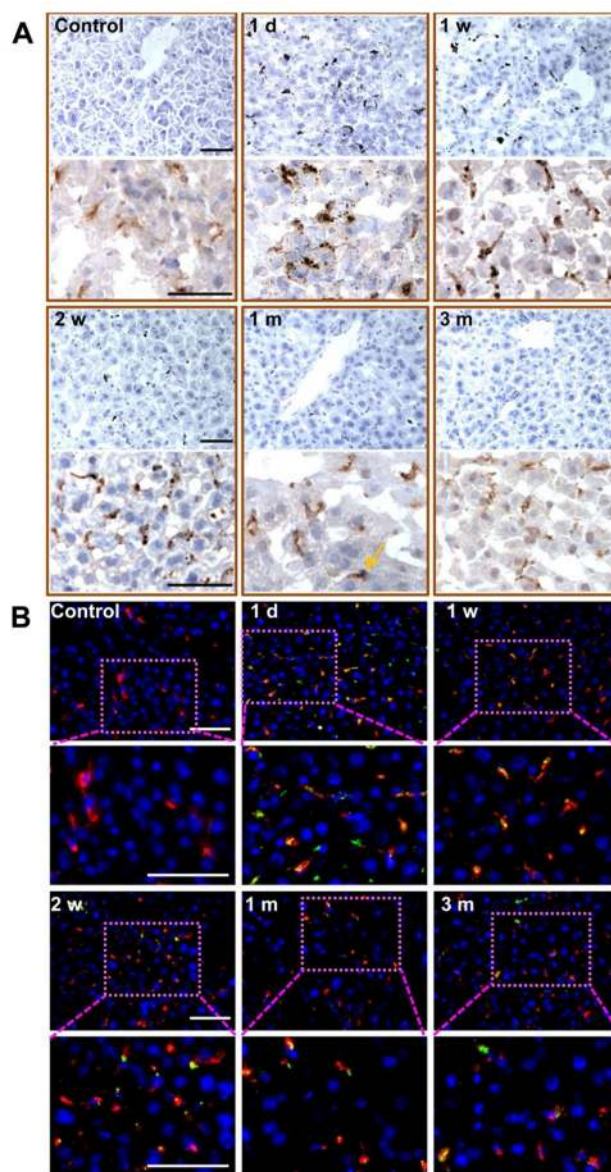
Figure 5.
Histological analysis of nanoparticles distribution in liver. (A), Distribution of CuS nanoparticles in liver. Black, CuS nanoparticles with sliver staining. Blue, cell nuclei counterstained with hematoxylin. Brown colored cells in lower image of each panel, Kupffer cells immunostained with rat anti-mouse CD68 antibody followed by peroxidase-goat anti-rat IgG and diaminobenzidine tetrahydrochloride (DAB) development. Bars, 50 μm. (B), Distribution of HAuNS in liver. Pseudo-green, scattering signal of HAuNS under dark field. Blue, DAPI-stained cell nuclei. Red, Kupffer cells immunostained with rat anti-mouse CD68 antibody followed by Alexa Fluor 549-conjugated goat anti-rat IgG. Bars, 50 μm.
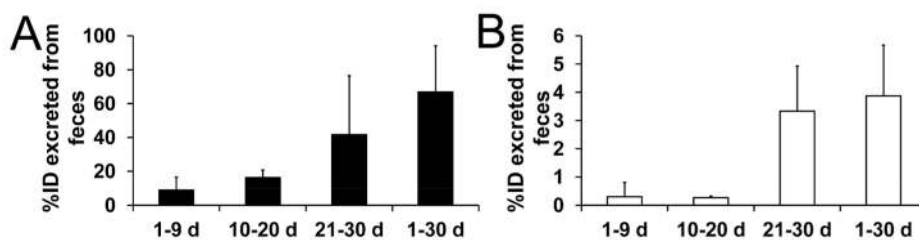
Figure 6.
The cumulative excreted Cu (A) and Au (B) in the feces from mice injected with PEG-HCuSNPs (20 mg/kg of Cu) or PEG-HAuNS (20 mg/kg of Au). The cumulative Cu or Au in the feces was collected at 1–9 d, 10–20 d and 21–30 d following administration, respectively. The amount of Cu or Au in "1–30 d" was the sum of these three consecutive time periods. %ID represents percentage of injected dose. Data are presented as mean ± standard deviation (n=3).
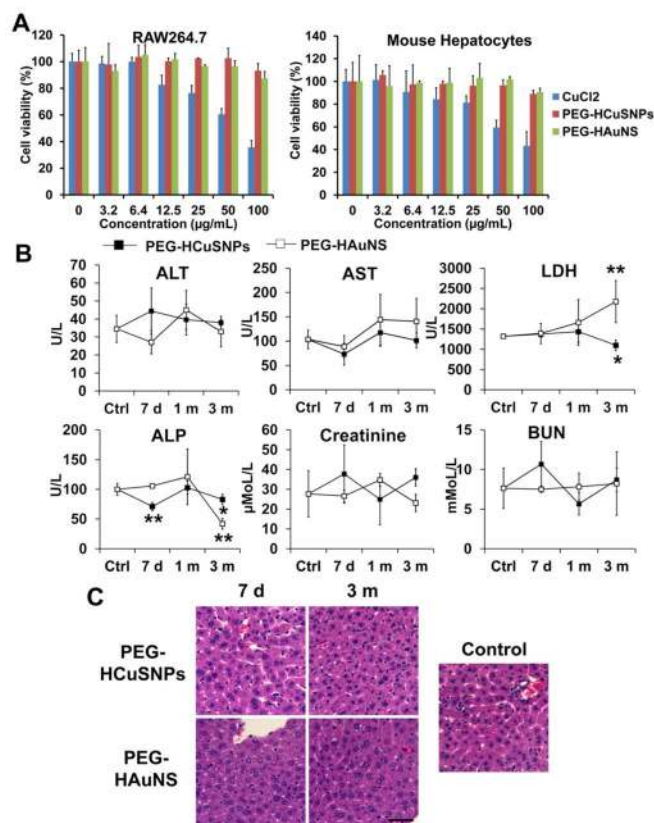
Figure 7.
(A), Viability of RAW264.7 cells and primarily cultured mouse hepatocytes exposed to different concentration of Cu or Au. For CuCl$_2$ and PEG-HCuSNPs treatment groups, X-axis represents the Cu concentration; for PEG-HAuNS treatment group, X-axis represents the Au concentration. Cell viability was measured by the MTT assay. Data are plotted as the percentage of viable cells compared to untreated controls. Each value represents mean ± standard deviation (n=4). (B), The mouse serum level of biochemical variables 7 d, 1 m, or 3 m after i.v. injection of PEG-HCuSNPs (20 mg/kg of Cu, filled boxes) or PEG-HAuNS (20 mg/kg of Au, open boxes). "Ctrl" represents mice without any treatment. Values are the means ± standard deviation, n = 5. Significant difference in the parameters between nanoparticle-treated groups and the control (*, $p < 0.05$; **, $p < 0.01$). ALT, alanine aminotransferase; AST, aspartate aminotransferase; LDH, lactate dehydrogenase; ALP, alkaline phosphatase; BUN, blood urea nitrogen. (C), H&E staining of mouse liver samples 7 d or 3 m following i.v. injection of PEG-HCuSNPs (20 mg/kg of Cu), or PEG-HAuNS (20 mg/kg of Au). Bars, 50 μm.
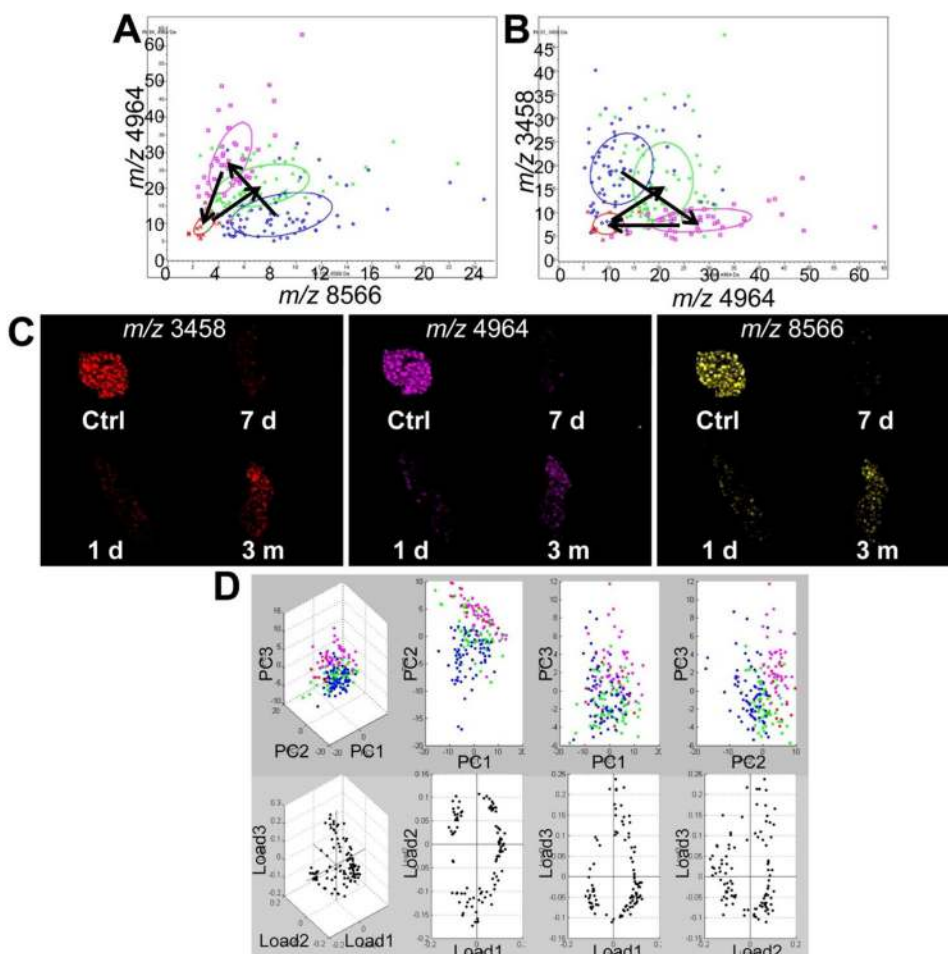
Figure 8.
MALDI-TOF IMS analysis of frozen liver slices from mice with or without i.v. injection of PEG-HCuSNPs (20 mg/kg of Cu). (A–B), 2-D peak distribution views (A) using p-value t-test ANOVA, significant peaks (pk186, 8566 Da; pk94, 4964 Da) and (B) using difference average, significant peaks (pk94, 4964 Da; pk51, 3458 Da). The liver tissues were collected at 1 d (pink), 7 d (red), or 3 m (green) after the injection. Blue, liver from mice without any treatment (Control). The axes show the peak area/intensity values with respect to the significant peaks. The ellipse represents 95% confidence interval. Arrows represent direction of disparity of the distributions over time. (C), Imaging of mass peaks in liver with significant difference between the nanoparticle-treated and untreated samples. Each represents the distribution of one peak with *m/z* noted in the tissue slice. (D), Scores (top row) and loading (bottom row) outputs of principal component analysis (PCA). During the calculation of the principal components (PCs), the variables (peaks) obtained different loadings in dependence on their contribution to the explained variance of a PC. Pink, 1 d; Red, 7 d; Green, 3 m; Control, blue.
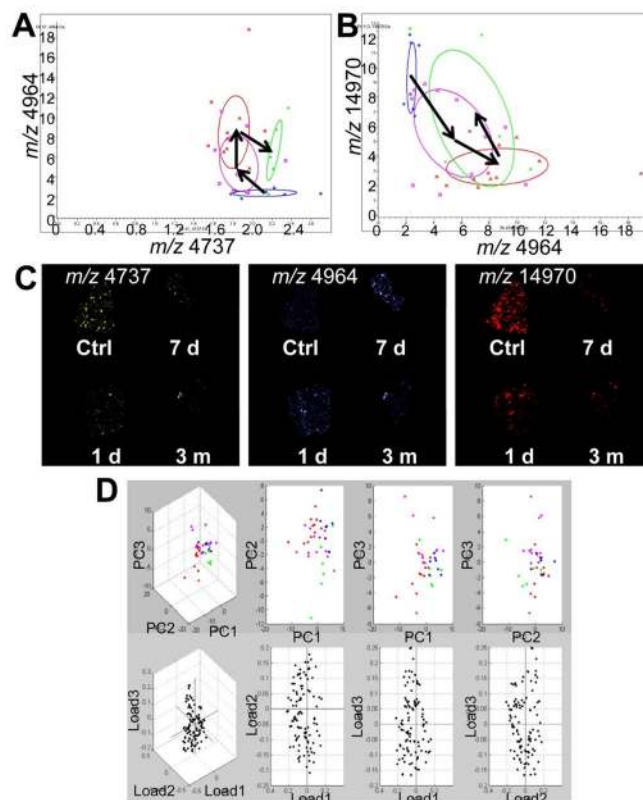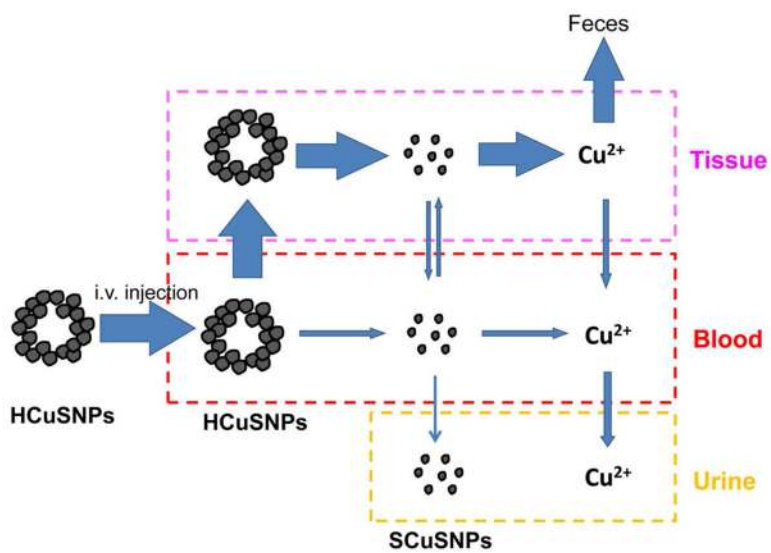
Figure 9.
MALDI-TOF IMS analysis of frozen liver slices from mice with or without i.v. injection of PEG-HAuNS (20 mg/kg of Au). (A–B), 2-D peak distribution views (A) using p-value t-test ANOVA, significant peaks (pk41, 4737 Da; pk47, 4964 Da) and (B) using difference average, significant peaks (pk47, 4964 Da; pk113, 14970 Da). The liver tissues were collected at 1 d (pink), 7 d (red), or 3 m (green) after the injection. Blue, liver from mice without any treatment (Control). The axes show the peak area/intensity values with respect to the significant peaks. The ellipse represents 95% confidence interval. Arrows represent direction of disparity of the distributions over time. (C), Imaging of mass peaks in liver with significant difference between the nanoparticle-treated and untreated samples. Each represents the distribution of one peak with *m/z* noted in the tissue slice. (D), Scores (top row) and loading (bottom row) outputs of principal component analysis (PCA). During the calculation of the principal components (PCs), the variables (peaks) obtained different loadings in dependence on their contribution to the explained variance of a PC. Pink, 1 d; Red, 7 d; Green, 3 m; Control, blue.

Scheme 1.
Illustration of disposition of HCuSNPs in body following i.v. injection.